Design of Multifunctional Gold Nanoparticles for *In Vitro* and *In Vivo* Gene Silencing

João Conde,[†,‡,¶] Alfredo Ambrosone,[§,¶] Vanesa Sanz,[†] Yulan Hernandez,[†] Valentina Marchesano,[§] Furong Tian,[⊥] Hannah Child,[∥] Catherine C. Berry,[∥] M. Ricardo Ibarra,[†] Pedro V. Baptista,[‡] Claudia Tortiglione,[§,*] and Jesus M. de la Fuente[†,*]

[†]Instituto de Nanociencia de Aragon, University of Zaragoza, C/Mariano Esquillor s/n Zaragoza, Spain, [‡]CIGMH, Departamento de Ciências da Vida, Faculdade de Ciências e Tecnologia, Universidade Nova de Lisboa, Campus de Caparica, 2829-516 Caparica, Portugal, [§]Istituto di Cibernetica "E. Caianiello", Consiglio Nazionale delle Ricerche (CNR), Via Campi Flegrei 34, Pozzuoli, Italy, [⊥]Comprehensive Pneumology Center, Institute of Lung Biology and Disease, Helmholtz Zentrum München, Munich, Germany, and [∥]Centre for Cell Engineering, University of Glasgow, Joseph Black Building, University Place, Glasgow, United Kingdom. [¶]These authors contributed equally to this work.

ABSTRACT Over the past decade, the capability of double-stranded RNAs to interfere with gene expression has driven new therapeutic approaches. Since small interfering RNA (siRNAs, 21 base pair double-stranded RNA) was shown to be able to elicit RNA interference (RNAi), efforts were directed toward the development of efficient delivery systems to preserve siRNA bioactivity throughout the delivery route, from the administration site to the target cell. Here we provide evidence of RNAi triggering, specifically silencing c-myc protooncogene, *via* the synthesis of a library of novel multifunctional gold nanoparticles (AuNPs). The efficiency of the AuNPs is demonstrated using a hierarchical approach including three biological systems of increasing complexity: *in vitro* cultured human cells, *in vivo* invertebrate (freshwater polyp, *Hydra*), and *in vivo* vertebrate (mouse) models. Our synthetic methodology involved fine-tuning of multiple structural and functional moieties. Selection of the most active functionalities was assisted step-by-step through functional testing that adopted this hierarchical strategy. Merging these chemical and biological approaches led to a safe, nonpathogenic, self-tracking, and universally valid nanocarrier that could be exploited for therapeutic RNAi.

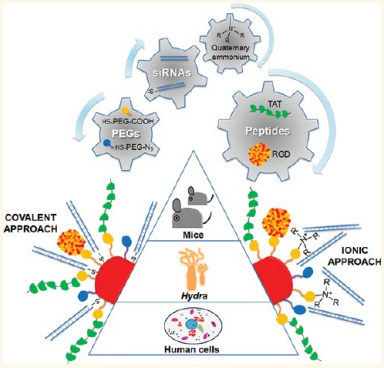

KEYWORDS: gold nanoparticles · RNA interference · animal models · biofunctionalization · c-myc · cancer

Nanoparticles exhibit excellent physicochemical properties for application in drug delivery, namely, their reduced sizes, rendering them capable of interacting with biomolecules in a one-to-one scale, and the high surface-to-volume ratio allowing for surface functionalization with a plethora of molecules for specific targeting and drug payloads.[1,2] Among the numerous nanoparticle formulations designed to improve siRNA[3,4] delivery and efficiency, those based on gold nanoparticles (AuNPs) have been extensively investigated without undesirable immune response or off-target effects.[5−15] To our knowledge, with the exception of one report on AuNPs for systemic administration of siRNA in humans,[16] over the last 6 years, formulations using AuNP-siRNA have solely been tested in cell cultures targeting reporter genes, such as luciferase or green fluorescence protein.[17] However, as with any drug treatment, gene therapy vehicles need extensive testing in archetypal animal models before translation into the clinics, and this requires the coordinated effort of interdisciplinary research groups.[18]

Here we used a functional comparative approach to assist the smart design, synthesis, and testing of a library of multifunctional nanodevices for RNAi, resulting in a nanocarrier based on AuNPs as the delivery system, with demonstrated functionality both *in vitro* and *in vivo* for RNAi-based therapy. Several biochemical moieties, cell penetrating and cell adhesion peptides were selected to enhance cellular recognition and uptake and confer specific downregulation of gene expression. The c-myc protooncogene, a key gene playing a pivotal role in cell cycle and tissue homeostasis,[19] was selected as RNAi target; poly(ethylene glycol) (PEG) molecules were incorporated to guarantee nanoparticle stability and avoid unspecific interactions, and three *in vitro*/*in vivo* model systems were selected: human cells (HeLa), freshwater polyps (*Hydra vulgaris*), and

* Address correspondence to c.tortiglione@cib.na.cnr.it, jmfuente@unizar.es.

Received for review July 6, 2012 and accepted August 12, 2012.

Published online August 12, 2012
10.1021/nn3030223

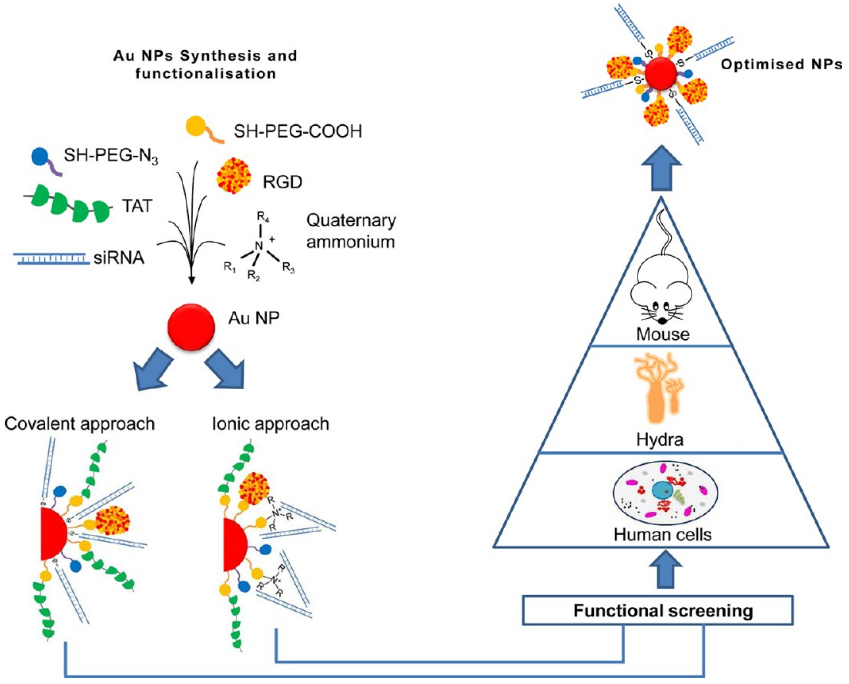

Figure 1. ***In vivo*** **gene silencing through nanoparticle-mediated RNAi. The nanocarrier is a AuNP functionalized with multiple biomolecules: PEG, cell penetration and cell adhesion peptides, and siRNA. Two different approaches were employed to conjugate the siRNA to the AuNP: (1) covalent approach, use of thiolated siRNA for gold−thiol binding to the nanoparticle; (2) ionic approach, interaction of the negatively charged siRNA to the modified surface of the AuNP through ionic interactions. A hierarchical scheme employed three biological systems of increasing complexity: cultured cells (HeLa), freshwater polyp (Hydra vulgaris), and mouse (C57BL/6j) to screen the synthesized nanocarrier library and select the ideal engineered AuNP for the delivery of siRNA to block gene function.**

mouse (C57BL/6j) (Figure 1). This chemical and biological strategy allowed us to compare the effect of the siRNA linkage to the NPs and the effect of cell penetration and adhesion peptides, finally leading to an optimally designed nanocarrier for RNAi therapeutic purposes.

RESULTS AND DISCUSSION

Stable AuNPs with an average diameter of 14 ± 1 nm were synthesized by reduction of sodium tetrachloroaurate(III) hydrate with sodium citrate dehydrate (Figure S1 of Supporting Information). To increase the stability, biocompatibility, and grant chemical functionality, AuNPs were functionalized with two types of thiolated poly(ethylene glycol) (PEG) spacers: a commercial carboxylated spacer, SH-EG(8)-$(CH_2)_2$-COOH, and an azide-containing spacer custom synthesized in our lab, SH-$(CH_2)_3$-CONH-EG(6)-$(CH_2)_2$-N_3. The carboxylated spacer provides the anchoring moieties for the covalent binding of amine-containing molecules through carbodiimide chemistry, while the azide-containing spacer confers positive *Z*-potential values, which is a crucial factor for cell uptake. Combined functionalization of the AuNPs with both spacers was finely tuned by controlling both specific spacer composition and degree of saturation (Figure S2). In order to elucidate the most efficient strategy to bond siRNA to AuNPs, two types of AuNPs stabilized by different degrees of PEG saturation were selected: (i) NP-ion with 100% coverage (25% azide-containing spacer and 75% carboxylated spacer); (ii) NP-cov with 25% coverage (50% of either spacer). These AuNP formulations represented the basic nanoparticles for downstream functionalization with c-myc siRNA, using either ionic interaction (ION) or covalent binding (COV). Both were initially tested for biocompatibility and toxicity in two human cancer cell lines (MCF-7 and HeLa). Cell survival rates following AuNP exposure were determined *via* MTT, with no cytotoxicity detected up to 48 h of incubation with either NP-ion or NP-cov (Figure S5). Further functionalization of these nontoxic AuNPs with c-myc siRNA and the HIV-derived TAT peptide was performed.[20] In the ION method, quaternary ammonium groups (R_4N^+) were bound to AuNPs through carbodiimide chemistry between the carboxylated spacer and (2-aminoethyl)trimethylammonium hydrochloride. Ionic interactions between the negatively charged siRNA backbone and both the azide and quaternary ammonium positively charged groups ensured binding of siRNA onto the NP surface for the whole pH range. In the COV method, thiolated siRNA was bound *via* a thiol bond to AuNPs with a nonsaturated PEG layer. The TAT peptide was bound to NP-ion and NP-cov by EDC/NHS coupling between the carboxylated spacer and the amine terminal group of the KKKGRKKRRQRRR (KKK-TAT) peptide. The binding efficiency of each functional group was determined by Bradford assay, alongside detailed

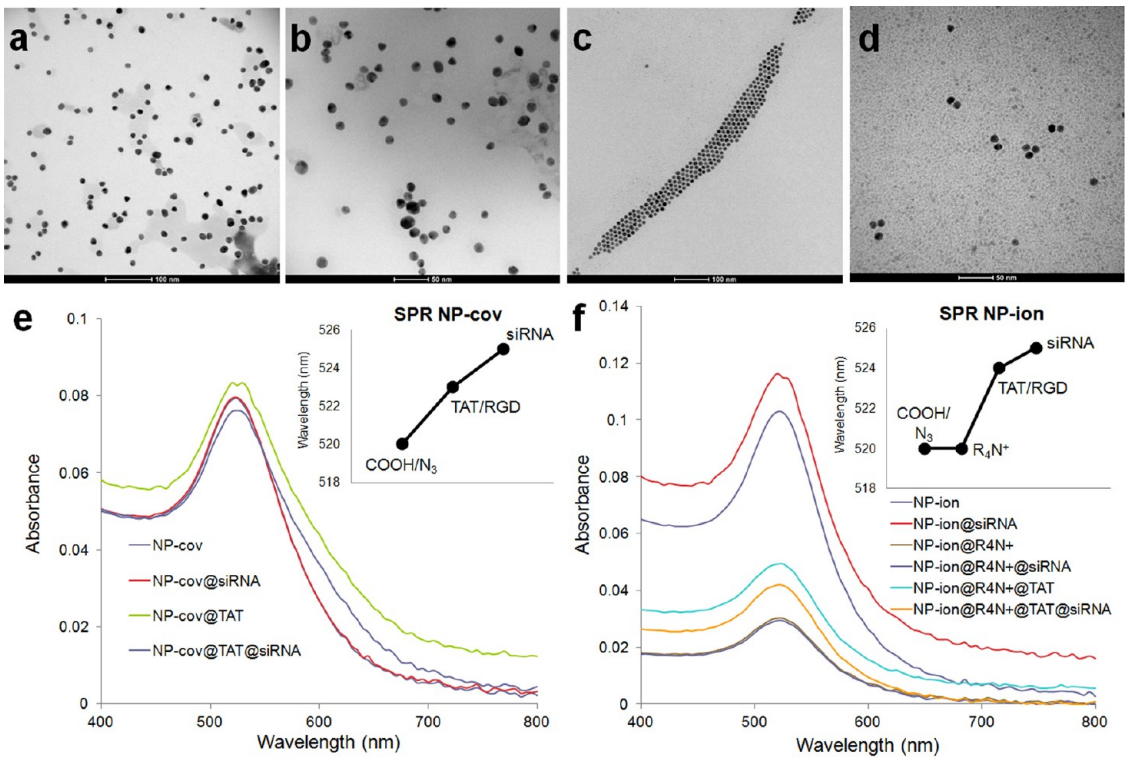

g AuNP conjugates	PEG chains/NP	TAT peptides/NP	RGD peptides/NP	siRNA strands/NP	Zeta Potential (mV)
NP-cov	1250.5±279.8	–	–	–	-38.3±3.5
NP-cov@siRNA	1250.5±279.8	–	–	41.3±0.8	-25.5±1.2
NP-cov@TAT@siRNA	1250.5±279.8	22.5±1.2	–	46.5±0.9	-39.1±0.7
NP-cov@TAT	1250.5±279.8	22.5±1.2	–	–	-26.1±0.9
NP-cov@RGD@siRNA	1250.5±279.8	–	20.6±0.7	62.9±0.8	-32.3±2.1
NP-ion	4783.8±349	–	–	–	-21.2±0.7
NP-ion@siRNA	4783.8±349	–	–	107.1±2.0	-14.5±0.9
NP-ion@R_4N^+@siRNA	4783.8±349	–	–	78.5±1.1	-7.7±1.0
NP-ion@R_4N^+	4783.8±349	–	–	–	4.3±1.1
NP-ion@ R_4N^+@TAT	4783.8±349	38.5±1.4	–	–	18.3±0.6
NP-ion@R_4N^+@TAT@siRNA	4783.8±349	38.5±1.4	–	76.1±2.1	-25.1±2.7
NP-ion@R_4N^+@RGD@siRNA	4783.8±349	–	12.7±1.1	45.6±1.4	-26.8±1.5

Figure 2. Physicochemical characterization of AuNPs. TEM analysis of (a) NP-cov@myc-siRNA, (b) NP-cov@TAT@myc-siRNA, (c) NP-ion@R_4N^+@myc-siRNA, (d) NP-ion@R_4N^+@TAT@myc-siRNA. The stabilization effect of the different functional groups on the multifunctional AuNPs can be observed *via* examination of the optical properties by UV−vis spectroscopy (e,f): absorption band of the resulting AuNPs appeared at ±520 nm due to the surface plasmon resonance (SPR) of the AuNPs. The spatial arrangement of AuNP can be inferred by measuring the shift of a characteristic SPR band dependent from size, shape, aggregation state, and medium polarity. The SPR of the AuNPs shown in e and f insets exhibited a red shift from 520 to 525 nm: a 3 nm shift for TAT/RGD peptides binding and a 5 nm shift for siRNA binding indicating successful binding of several groups. (g) Quantification of the PEG chains, TAT and RGD peptides, and siRNA strands is shown for all bioconjugates, together with the *Z*-potential measurements.

AuNP assay characterization (Supporting Information). All AuNP bioconjugates presenting at the surface siRNA and/or TAT/RGD and/or quaternary ammonium groups (R_4N^+) in various combinations were characterized by transmission electron microscopy (TEM), UV/vis spectroscopy, surface plasmon resonance (SPR) shift, and zeta-potential (see Figure 2). To determine cell uptake and intracellular fate, HeLa cells were incubated with the functionalized AuNPs for 18 h and processed for TEM analysis. Results show that both NP-ion and NP-cov conjugates were found isolated or as small aggregates in the cytoplasm (Figure 3b,c).

To permit rapid screening of the large variety of functionalized AuNPs in terms of c-myc RNAi, the c-myc gene sequence was cloned into a psiCHECK-2 vector downstream of the Renilla luciferase reporter (Figure S4). This construct was stably expressed in HeLa cells, and the decrease in luciferase activity, as consequence of RNAi, was quantified by a luminescence assay. Figure 3d shows normalized luciferase activity of each AuNP conjugate, where both synthetic approaches used to bind siRNA onto the AuNP (ION *versus* COV) show comparable silencing efficiency, matching that attained *via* the transfection of naked siRNA with lipofectamine. Control experiments utilized

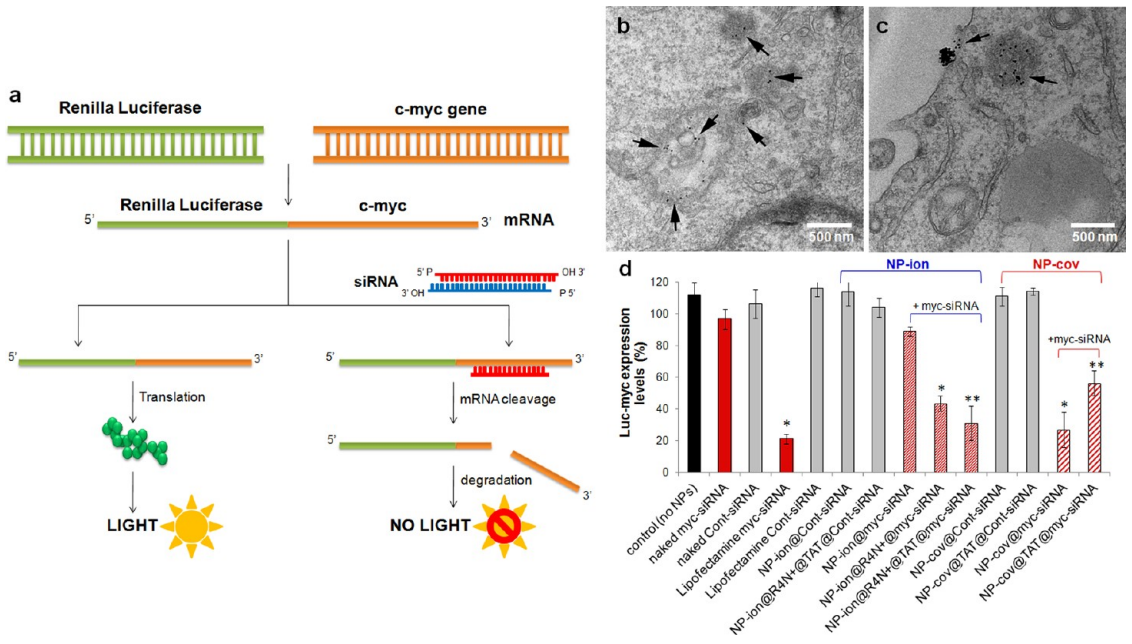

Figure 3. Internalization and efficiency of c-myc RNAi induced by functionalized AuNP in HeLa cells. (a) Renilla luciferase was used as the primary reporter gene, and the c-myc gene was cloned into a multiple cloning region located downstream of the Renilla gene. Initiation of the RNAi process by synthetic myc-siRNAs results in cleavage and subsequent degradation of the fusion mRNA. Measuring decreases in Renilla activity provides a convenient way of monitoring the RNAi effect. This vector also contains a second reporter gene, Firefly luciferase, which functions as an internal control for reporter gene activity (scheme adapted from Promega psiCHECK vectors). (b,c) TEM images of cells treated with NP-cov@myc-siRNA (b) and NP-ion@myc-siRNA (c) show NPs present in the cytoplasm as single units, supporting the correct delivery of siRNA to initiate RNAi. (d) Quantitative assessment of RNAi efficiency. HeLa cells were transfected with the recombinant vector psiCHECK-2, encoding for the fusion protein Renilla luciferase-myc. Decrease of Renilla luciferase activity induced by c-myc-siRNA was expressed as percentage of normal luciferase activity. Unrelated siRNA (cont-siRNA) bound on the AuNPs; naked or lipofectamine delivered siRNA were included as negative and positive RNAi controls, respectively. Data marked with asterisks are statistically significant relative to the corresponding NP-ion/cov with control siRNA as calculated by paired Sample *t* test (, $P \leq 0.0001$; *, $P \leq 0.001$).**

a nonrelated siRNA (cont-siRNA) that does not induce downregulation of luciferase or c-myc. These results clearly show the effective capability of the functionalized AuNPs to specifically and selectively silence c-myc gene expression. With regard to NP-ion design, Figure 3d depicts the importance of including R_4N^+ moiety to introduce ionic interactions between the positively charged NPs and the negatively charged siRNA. Absence of R_4N^+ did not induce any silencing, suggesting a possible proton-sponge effect played by the carboxylic and quaternary ammonium groups, which could be responsible for endosome rupture and release of the trapped materials (siRNA) into the cytoplasm.[21] Also, addition of the TAT peptide branched on NP-ion@R_4N^+@myc-siRNA showed negligible effects when compared to the same NP without TAT, probably due to steric hindrance of siRNA. Concerning the NP-cov@myc-siRNA, their efficiency in achieving RNAi might result from increased stability of the siRNA covalently bound to the gold core compared to their stability when adsorbed by electrostatic interaction on the NP surface. However, the possibility that the strong efficiency of this adduct might depend on cytoplasmic release of the siRNA (due to the reducing environment of the cytoplasm acting on the thiol bonds) and prompt availability to trigger the RNAi machinery cannot be excluded. When branched on NP-cov@myc-siRNA, the TAT peptide again decreased the RNAi efficiency from 73 ± 11 to 43 ± 7%. These data support the hypothesis that the TAT peptide may act as a suppressor of the RNAi response, as previously reported,[22] which might be related to the fact that this virally derived peptide has evolved to naturally bypass cell defense mechanisms. In summary, despite the low AuNP concentration used (2.1 nM AuNPs, 2 pM siRNA), following confirmed cell uptake *via* TEM (Figure 3b,c), it was able to trigger a very efficient RNAi, likely due to the amplification of the siRNA signal *in vivo*, as elsewhere reported.[23]

Prior to testing the efficiency of the multifunctional nanocarrier for c-myc RNAi on an archetypal animal model, we used a simpler and more singular invertebrate model, *Hydra vulgaris* (Cnidaria, Hydrozoa), to allow for further fine-tuning of the nanocarrier. Thus, following successful silencing in the cell model, the efficiency of both NP-ion and NP-cov were evaluated in the *Hydra in vivo* model. The increase in complexity of the animal model, in fact, could enable us to select the more appropriate nanocarrier to test in mouse. *Hydra* is a freshwater polyp whose structural anatomy reflects a tissue grade of organization (body composed of two cell layers; absence of either proper organs, or central

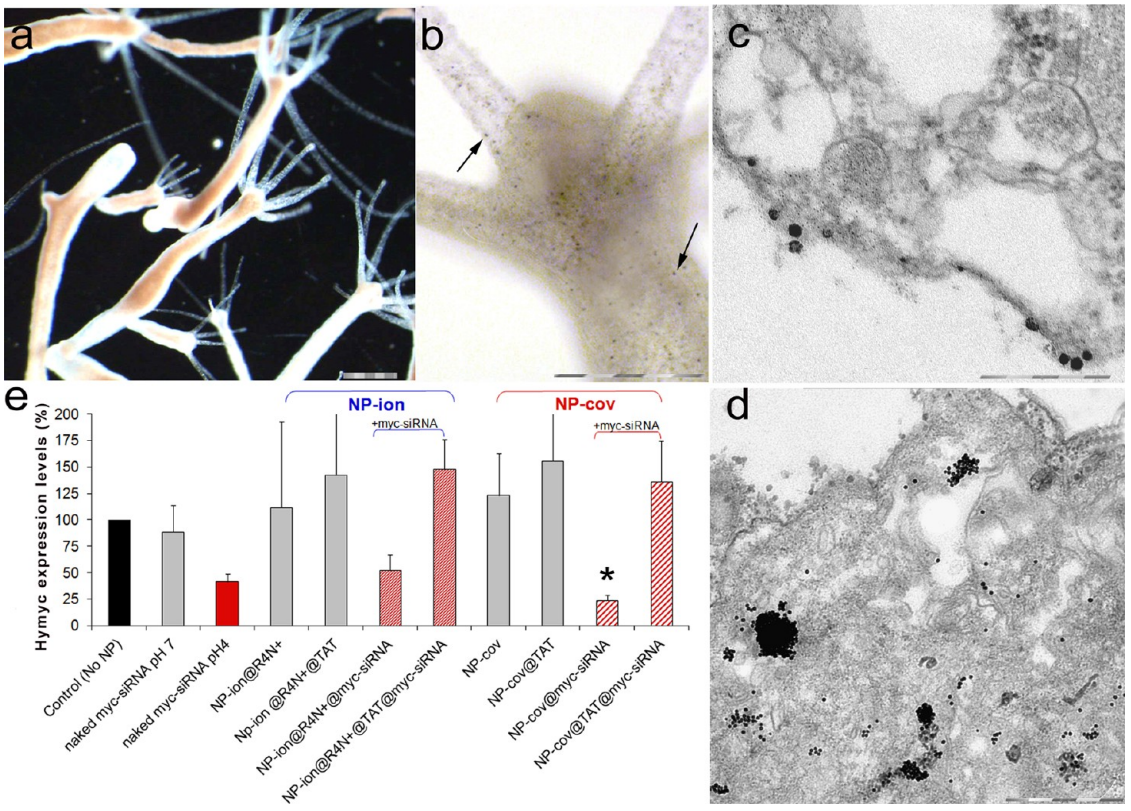

Figure 4. Hymyc RNAi in Hydra vulgaris. (a) Representative images of living polyps of Hydra vulgaris (scale bar 0.5 mm). (b) Bright-field image of Hydra treated 24 h with NP-cov@myc-siRNA (scale bar 200 μm). Nanoparticles appear as dark spots on the Hydra ectodermal cells. Same uptake was observed for NP-ion@myc-siRNA (Supporting Information Figure S3). (c,d) TEM images of Hydra tissues, prepared from polyps treated with 15 nM of NP-cov@myc-siRNA for 30 min (c) and 24 h (d). NPs are detected as single unit or small clusters into the cytoplasm for correct delivery of siRNA. Scale bar: 0.2 μm (c) and 0.5 μm (d). (e) Molecular assessment of RNAi efficiency by qRT-PCR using 15 nM AuNPs and 25 polyps in 100 μL of Hydra medium. Hymyc relative expression upon incubation with NP-ion and NP-cov was compared to naked siRNA. Relative gene expression changes from NPs not carrying c-myc siRNA are shown as gray bars, while those induced by Hymyc siRNA functionalized NPs are colored red. Data are means of three independent experiments from three biological replicates; error bars show standard deviation. Data marked with asterisk are statistically significant relative to the corresponding NP-ion/cov without siRNA as calculated by paired sample *t* test (*, $P \leq 0.005$).

nervous system), but exhibiting behavior and physiology proper of animals (Figure 4a and Figure S6 of Supporting Information). Reliable methods have been developed for a comprehensive analysis of nanoparticle impact in *Hydra*, spanning from *in vivo* analysis induced by nanoparticle treatments (structural morphological changes, impact on reproductive rate, efficiency of regeneration) to *in vitro* approaches of cell biology, microscopy, and molecular biology to investigate the internalization routes and the genotoxic effects.[24,25]

Moreover, the *Hydra c-myc* (Hymyc) homologue gene function has been recently identified,[26,27] allowing to functionally test the RNAi efficiency. NP-ion and NP-cov were initially tested for biocompatibility and toxicity by measuring the impact on population growth rate,[25] showing the absence of toxic effects (Figure S7). Optical microscopy showed that both NP-ion and NP-cov were internalized at low rate by ectodermal cells, facing the animal outer plane (Figure 4b and Figure S3), and TEM analysis was necessary for subcellular localization of AuNPs. In Figure 4c, TEM images on thin sections from animals incubated 30 min with NP-cov@myc-siRNA show nanoparticles bound to the membrane glycocalix, as single units or small clusters passing through the bilayer structure of the cell membrane. After 24 h of incubation, AuNPs were found in the cytoplasm, clustered or monodispersed, demonstrating their capability to cross biological membranes and shuttle siRNA into the cytoplasm (Figure 4d). Hymyc silencing efficiency was assessed using the AuNPs recommended following HeLa silencing (NP-ion@R_4N^+@myc-siRNA, NP-ion@R_4N^+@TAT@myc-siRNA, NP-cov@TAT@myc-siRNA, NP-cov@myc-siRNA). The qRT-PCR results in *Hydra* further restricted the selection of bioactive AuNP conjugates previously identified in HeLa cells: only two of those nanoparticles induced Hymyc gene silencing, NP-ion@R_4N^+@myc-siRNA and NP-cov@myc-siRNA, which rise up to 80% of gene downregulation in the case of the covalent conjugate (Figure 4e). TAT peptide (initially employed to enhance the cell permeability), but causing a decrease in the RNAi efficiency of the NP-cov conjugates in HeLa cells, completely inhibited

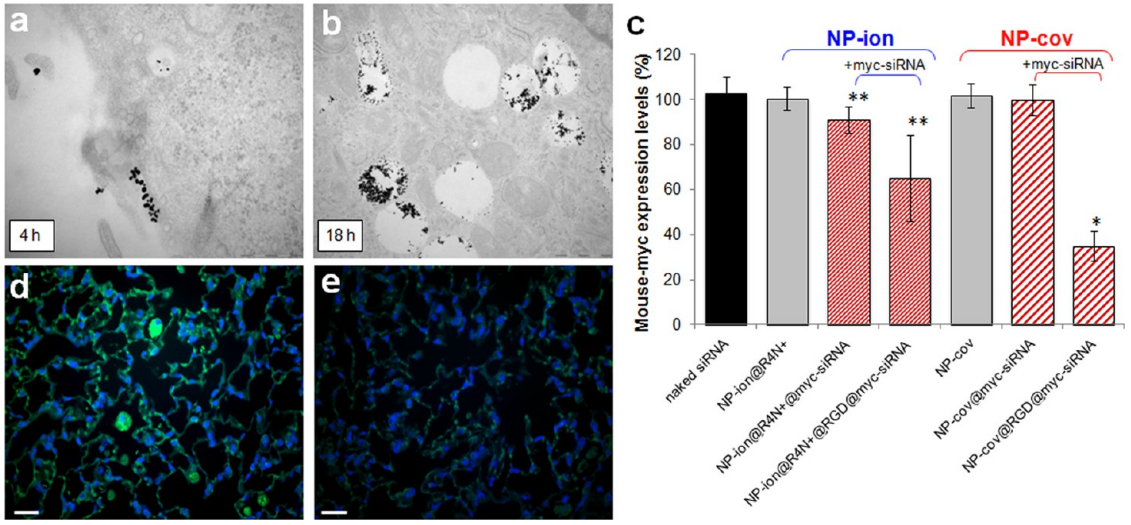

Figure 5. c-myc RNAi in mouse. (a,b) TEM images of lung epithelial cells. Mice (C57BL/6j strain) were treated with 16 nM of NP-cov@RGD@myc-siRNA by intratracheal instillation. At 4 h (a) after instillation, NPs are located in ruffles of lung epithelial cell membranes and a few NPs are in the vesicles. At 18 h (b), huge amounts of NPs are found in vesicles or free in cytoplasm (scale bars 500 nm). (c) Molecular assessment of RNAi efficiency. To quantify efficiency of silencing, total RNAs from lung tissue (four mice treated with each NP type) were extracted after 48 h and analyzed by qRT-PCR. The c-myc expression levels were determined using β-actin as reference gene. Data marked with asterisks are statistically significant relative to the corresponding NP-ion/cov without siRNA as calculated by paired sample *t* test (*, $P \leq 0.001$; **, $P \leq 0.01$). (d,e) c-myc protein expression on alveolar epithelial cells in lung tissue after 48 h treatment. (d) Mice instillated with 16 nM NP-cov@RGD, (e) mice instillated with 16 nM NP-cov@RGD@myc-siRNA. The c-myc protein was detected by Alexa-488-conjugated anti-c-myc antibody (green), and cell nuclei were DAPI stained (blue). Scale bars 200 μm.

the RNAi process in *Hydra*, further suggesting that TAT RNAi suppressor activity may be conserved throughout the animal kingdom.[22] Those AuNPs unable to induce gene silencing in cells were also ineffective in *Hydra*, confirmed by analysis of gene expression (Figure 4e).

Finally, the two AuNPs identified as inducing c-myc silencing in both HeLa and *Hydra*, NP-ion@R_4N^+@myc-siRNA and NP-cov@myc-siRNA, were tested in the more complex *in vivo* mouse model. Both AuNPs were administered to 10−12 week aged female mice (n = 6−8 animals) by intratracheal instillation. While intravenous administration is the most popular choice in clinical studies, an oral route inhalation or intratracheal instillation mode, together with intranasal drug delivery, convection-enhanced diffusion, and intrathecal/intraventricular drug delivery systems has been gaining considerable attention. Intratracheal instillation of nanoparticles becomes an important criterion of consideration to overcome the physiological barriers of the lung and to achieve locally high drug concentrations for pulmonary diseases. In our case, the choice was also dictated by the siRNA loaded on the AuNP, targeting the c-myc gene. As this oncogene is deregulated in lung cancer, in a future study of lung cancer treatment, this administration mode might allow proper deliver of therapeutic siRNA to the target organ. After 7 days from instillation, mice were dissected for bronchoalveolar lavage (BAL cells) and lung tissue extraction. In general, NPs of size <100 nm and different zeta-potential display toxic effects, due to trade-off between drug potency and immunologic surveillance.[28,29] In fact, the influence of size, solubility, and surface modification on the biocompatibility of nanoparticles and their use in biological applications is well-known. NPs have a proclivity *in vivo* and *in vitro* to bioaccumulate within various types of cells with a special affinity for macrophage-type cells and reticuloendothelial cells throughout the body. In order to select safe material for drug delivery, toxicity studies of both NP-cov and NP-ion sets were performed in mice following 1, 3, and 14 days of treatment by the evaluation of the number of macrophages, neutrophils, and lymphocytes, in which an increase indicates an inflammation process. Results showed negligible adverse effects using a low instillation dose (16 nM) (Supporting Information, Figure S8). However, the qRT-PCR performed on four lung samples of each groups, instilled with this dose of NPs, showed very low gene downregulation (Figure 5c), probably due to a lack of NPs' selectivity to the target cells. The functional studies performed in *in vitro* cell culture and in living *Hydra* provided feedback for improving the design and synthesis of AuNPs@siRNA targeting mouse. To this aim, the cell adhesion peptide RGD was incorporated on the AuNP to reinforce cell−NP interaction and drive lung-specific uptake. RGD integrin ligand is well-known for its capability to bind to the integrin $\alpha_v\beta_3$ receptor family,[30] involved in a wide range of cell−extracellular matrix and cell−cell interactions. Previous studies have demonstrated RGD efficiency to promote NP−cell adhesion events.[31] RGD-containing peptides were conjugated to both NP-ion and NP-cov,

in the presence or absence of c-myc siRNA, by EDC/NHS coupling between the carboxylated spacer and the primary amine in the RGD peptide (Supporting Information). Mice were treated as previously indicated. TEM analysis on lung epithelial cells revealed the efficient uptake of NPs conjugated with RGD with sufficient cytoplasmic availability (Figure 5a,b) to initiate RNAi. The qRT-PCR results showed a 65.2 ± 6.7% c-myc downregulation induced by NP-cov@RGD@myc-siRNA and 34.9 ± 19% c-myc silencing by NP-ion@R_4N^+@RGD@myc-siRNA. These results confirm the specificity of the RNAi approach. Immunolocalization of the MYC protein on alveolar epithelial cells in lung tissue from mice treated with NP-cov@RGD@myc-siRNA confirmed decreased MYC protein accumulation in lung tissue, unequivocally demonstrating the bioactivity of the multifunctional NP (Figure 5d,e).

Remarkably, the same NP-cov@siRNA adduct was shown to elicit highest RNAi in HeLa cells, *Hydra vulgaris*, and mouse, with the only exception of the RGD presence when testing on mouse, as it is not expressed in *Hydra*. From an evolutionary point of view, having found that gene silencing in this primitive animal is accomplished by the same nanocarrier working on human cell cultures and mouse, underlines not only the conservation of key molecular pathways throughout animal evolution but also the conservation of the basic chemicophysical interactions between nanoparticle and the living world, *Hydra* bridging the gap between cell cultures and complex models.

CONCLUSION

In this study, we show that two balanced formulations (ionic and covalent approaches), in terms of stability/electrostatic interactions, designed to produce smart multifunctional nanostructures succeeded to generate new innovative and versatile tools for efficient RNA interference in eukaryotic systems. Using three biological models of increasing complexity (cultured cells, invertebrate, and mammal), both design and validation of multifunctional nanocarriers capable of selectively and specifically delivering siRNA *in vivo* were demonstrated. This functional screening approach allowed us to finely tune concentrations, bonding, and the combination of different chemical groups on the nanoparticle surface, addressing current ethical issues on unnecessary, cost-effective, and time-consuming vertebrate testing. These multifunctional nanocarriers are robust enough to preserve stability without showing acute toxicity or cell viability impairment while simultaneously able to bypass biological barriers to perform RNAi activity without off-target effects. Our universal nanocarrier represents a valid gene delivery platform that can be exploited for clinical application in the near future. While treatment of a lung cancer mouse model might represent the first therapeutic test of the nanocarrier developed here, the simple change of the siRNA sequence might target the same device to a huge range of diseases, strengthening the way to clinical application of RNAi.

METHODS

We divided the methods into similar parts for each system (except for the synthesis). Full description of methods can be found in Supporting Information.

Synthesis and Functionalization of Gold Nanoparticles. AuNPs with a diameter of 14 ± 1 nm were synthesized by the citrate reduction method described by Lee and Meisel.[32] A mixture of AuNPs, 0.028% SDS, and SH-EG(8)-$(CH_2)_2$-COOH (Iris-Biotech) and SH-$(CH_2)_3$-CONH-EG(6)-$(CH_2)_2$-N_3 in the adequate ratio for NP-ion and NP-cov was mixed under basic conditions for 16 h. PEGylated AuNPs were obtained after purification by centrifugation. Number of PEG molecules was carried out by Ellman's method. Further chemical functionalization with quaternary ammonium ((2-aminoethyl)trimethylammonium chloride hydrochloride), TAT, and RGD peptides was carried out by EDC (1-ethyl-3-(3-dimethylaminopropyl)carbodiimide) (Sigma) and sulfo-NHS (sulfo-hydroxysuccinimide) (Sigma) chemistry at pH 6.1 (25 mM MES). Quantification of TAT peptides was obtained by Bradford assay (CA). AuNP functionalization with siRNA (Thermo Scientific Dharmacon) was taking place using unmodified siRNA for NP-ion by mixing them with NP-ion@R_4N^+@TAT during 16 h at 4 °C. For NP-cov, thiolated siRNA was incubated with NP-cov@TAT containing 0.028% SDS and 0.1 M NaCl. Excess siRNA was removed by centrifugation at 4 °C. siRNA quantification was carried out by fluorescence measurement (Perkin-Elmer LS55) using a GelRed (Biotium) acid nucleic intercalator (see Supporting Information, Table 1, for siRNA sequences).

Hydra Culturing. *Hydra vulgaris* (strain Zurich, originally obtained by P. Tardent) were asexually cultured in Hydra medium (1 mM $CaCl_2$, 0.1 mM $NaHCO_3$, pH 7). The animals were kept at 18 ± 1 °C and fed three times per week with freshly hatched *Artemia salina* nauplii. *In vivo* imaging was accomplished at several magnifications by using both a stereomicroscope and an inverted microscope (Axiovert 100, Zeiss).

Transmission Electron Microscopy. To visualize the cellular uptake of NPs, HeLa cells were incubated with all NPs for 18 h. Mice were treated with NPs for 4 and 18 h. Mice were sacrificed and mice lungs fixed in 2.5% glutaraldehyde for TEM. For *Hydra*, polyps were treated with 2% urethane in Hydra medium and then fixed for 2 h in 2% glutaraldehyde in Hydra medium. Samples were postfixed in 1% buffered OsO_4 followed by 0.5% uranyl acetate for 1 h and then taken through alcohol dehydration increments and left in resin (propylene oxide Epon 812 resin mix (1:1) for cells and propylene oxide/Epon 12 resin mix (1:1) for *Hydra*) overnight. Cell layers were captured in pure resin and cured overnight in an oven. *Hydra* were incubated 2 × 2 h in Epon 12 resin. Blocks were then cut into ultrathin sections, stained with 2% methanolic uranyl acetate and Reynolds lead citrate, and viewed under a Leo 912 AB TEM (120 kV for cells and 80 kV for *Hydra*).

Toxicity. Cellular cytotoxicity was assessed by standard MTT assay (Invitrogen). *Hydra* growth rate was calculated to monitor NP toxicity, as previously described.[25] Toxicity in mice was assessed by enumeration of total differential cells in bronchoalveolar lavage cells. Several nanomaterials studied in the size range from *ca.* 5 to 20 nm (TiO_2, Fe, Cu, Ag) induced higher neutrophil recruitment in BAL fluid, compared to control.[33] Low amounts of neutrophiles and lymphocytes indicate minimal inflammatory response or toxicity.

Assessment of RNAi in HeLa Cells. c-myc RNAi was evaluated by using the psiCHECK Vector system (Promega), which allows one to monitor change in expression of a reporter gene (Luciferase) fused to a target gene. **MYC-Luciferase vector construction:** the whole human v-myc myelocytomatosis viral oncogene homologue (c-myc) gene was PCR amplified from cDNA retrotranscribed from HeLa cells total RNA (see Supporting Information) and the resulting product cloned in frame with Luciferase reporter gene contained into the vector psiCHECK-2, and maintained in *Escherichia coli* DH5α strains. **Cell culture:** HeLa cells were grown in Dulbecco's modified Eagle's medium (DMEM, Lonza) with 10% heat inactivated fetal bovine serum, 2 mM glutamine, 100 U/mL penicillin, and 100 μg/mL streptomycin and maintained at 37 °C in 5% CO_2. Cells were seeded at a density of 5×10^3 cells/well in 96-well plates and grown for 1 day prior to transfection of the MYC-Luciferase vector (0.125 μg per well) using Lipofectamine 2000 (Invitrogen) and Opti-MEM reduced serum medium (Invitrogen) according to the manufacturer's recommendations. RNAi efficiency of different NP conjugates (2.1 nM AuNPs, 2 nM siRNA) was tested by treating the cells for 48 h and by quantification of luciferase expression using a dual-luciferase reporter assay (Promega) assay according to the manufacturer's protocols. Data are average (±SD) of three experiments.

RNAi Experiments in Hydra. Groups of 10 animals, collected in plastic multiwells, were incubated in 100 μL of Hydra medium in the presence of AuNPs (15 nM), and the treatment was renewed after 24 h to account for possible siRNA degradation. At 48 h, animals were washed and processed for RNA extraction and qRT-PCR. Animals interfered by naked siRNA, nonfunctionalized NP, or untreated were used as controls. Briefly, total RNAs were purified using Trizol (Invitrogen), retrotranscribed using SuperScript II retrotranscriptase (Invitrogen), and used for qRT-PCR analysis (see Supporting Information for detailed methods and primers employed).

RNAi Experiments in Mouse. C57BL/6J mice were anesthetised by intraperitoneal injection of a mixture of Medetomidin (0.5 mg/kg body mass), Midazolam (5.0 mg/kg body mass), and Fentanyl (0.05 mg/kg body mass). The animals were then intubated by a nonsurgical technique. Using a cannula inserted 10 mm into the trachea, a suspension containing 16 nM AuNP in 50 μL of pyrogene-free distilled water was instilled, followed by 100 μL of air. After instillation, animals were antagonized by subcutaneous injection of a mixture of Atipamezol (2.5 mg/kg body mass), Flumazenil (0.5 mg/kg body mass), and Naloxon (1.2 mg/kg body mass) to guarantee their awakening and well-being. Animals were treated humanely and with regard for alleviation of suffering; experimental protocols were reviewed and approved by the Bavarian Animal Research Authority.

Preparation of BAL Cells/Fluid. BAL fluid was obtained by injecting and recovering of two 0.5 mL aliquots of PBS *via* a tracheal cannula. Cells in the lavage fluids were counted using a hemocytometer, and the differentials were determined by utilizing light microscopy to count 200 cells on cytospin preparations.

Molecular Analyses of Gene Expression in Mouse. Immunolocalization: Lung tissues were sliced and blocked by adding 1% BSA in PBS for 30 min. Mouse anti-c-myc (Molecular Probes) was added (dilution 1:1000) for 1 h, washed in PBS with agitation for 5 min three times, and incubated with goat anti-mouse IgG coupled with Alexa-488 (Molecular Probes) at 2 μg/mL for 30 min. Nuclei were DAPI stained before slide mounting with 50 μL of fluormount mounting medium. Total RNAs were extracted from mouse lungs, retrotranscribed, and analyzed by qRT-PCR (see Supporting Information for detailed methods and primers employed).

Conflict of Interest: The authors declare no competing financial interest.

Acknowledgment. Authors thank ERANET-NANOSCIERA NANOTRUCK project for financial support. We thank A. Tino, G. Estrada, V. Grazu, and P. del Pino for fruitful discussions. Authors thank I. Echaniz, S. Rivera, and G. Marino for technical support. J.M.F. thanks ARAID for financial support. P.V.B. thanks CIGMH. J.C. acknowledges FCT Grant SFRH/BD/62957/2009. A.A., V.M., and F.T. were granted by NANOTRUCK.

Supporting Information Available: Synthesis, physicochemical characterization, and functionalization of AuNPs; internalization of AuNP conjugates; evaluation of RNAi efficiency by functional reporter gene assay; evaluation of toxicity. This material is available free of charge *via* the Internet at http://pubs.acs.org.

REFERENCES AND NOTES

1. Sperling, R. A.; Parak, W. J. Surface Modification, Functionalization and Bioconjugation of Colloidal Inorganic Nanoparticles. *Philos. Trans. R. Soc, A* **2010**, *368*, 1333–1383.
2. Dreaden, E. C.; Alkilany, A. M.; Huang, X.; Murphy, C. J.; El-Sayed, M. A. The Golden Age: Gold Nanoparticles for Biomedicine. *Chem. Soc. Rev.* **2012**, *41*, 2740–2779.
3. Fire, A.; Xu, S.; Montgomery, M. K.; Kostas, S. A.; Driver, S. E.; Mello, C. C. Potent and Specific Genetic Interference by Double-Stranded RNA in *Caenorhabditis elegans*. *Nature* **1998**, *391*, 806–811.
4. Elbashir, S. M.; Harborth, J.; Lendeckel, W.; Yalcin, A.; Weber, K.; Tuschl, T. Duplexes of 21-Nucleotide RNAs Mediate RNA Interference in Cultured Mammalian Cells. *Nature* **2001**, *411*, 494–498.
5. Pecot, C. V.; Calin, G. A.; Coleman, R. L.; Lopez-Berestein, G.; Sood, A. K. RNA Interference in the Clinic: Challenges and Future Directions. *Nat. Rev. Cancer* **2011**, *11*, 59–67.
6. Shahzad, M. M.; Mangala, L. S.; Han, H. D.; Lu, C.; Bottsford-Miller, J.; Nishimura, M.; Mora, E. M.; Lee, J. W.; Stone, R. L.; Pecot, C. V.; *et al.* Targeted Delivery of Small Interfering RNA Using Reconstituted High-Density Lipoprotein Nanoparticles. *Neoplasia* **2011**, *13*, 309–319.
7. Giljohann, D. A.; Seferos, D. S.; Daniel, W. L.; Massich, M. D.; Patel, P. C.; Mirkin, C. A. Gold Nanoparticles for Biology and Medicine. *Angew. Chem., Int. Ed.* **2010**, *49*, 3280–3294.
8. Giljohann, D. A.; Seferos, D. S.; Prigodich, A. E.; Patel, P. C.; Mirkin, C. A. Gene Regulation with Polyvalent siRNA Nanoparticle Conjugates. *J. Am. Chem. Soc.* **2009**, *131*, 2072–2073.
9. Guo, S.; Huang, Y.; Jiang, Q.; Sun, Y.; Deng, L.; Liang, Z.; Du, Q.; Xing, J.; Zhao, Y.; Wang, P. C.; *et al.* Enhanced Gene Delivery and siRNA Silencing by Gold Nanoparticles Coated with Charge Reversal Polyelectrolyte. *ACS Nano* **2010**, *4*, 5505–5511.
10. Lee, Y.; Lee, S. H.; Kim, J. S.; Maruyama, A.; Chen, X.; Park, T. G. Controlled Synthesis of PEI-Coated Gold Nanoparticles Using Reductive Catechol Chemistry for siRNA Delivery. *J. Controlled Release* **2011**, *155*, 3–10.
11. Song, W. J.; Du, J. Z.; Sun, T. M.; Zhang, P. Z.; Wang, J. Gold Nanoparticles Capped with Polyethyleneimine for Enhanced siRNA Delivery. *Small* **2010**, *6*, 239–246.
12. Oishi, M.; Nakaogami, J.; Ishii, T.; Nagasaki, Y. Smart PEGylated Gold Nanoparticles for the Cytoplasmic Delivery of siRNA To Induce Enhanced Gene Silencing. *Chem. Lett.* **2006**, *35*, 1046–1047.
13. Moon, J. H.; Mendez, E.; Kim, Y.; Kaur, A. Conjugated Polymer Nanoparticles for Small Interfering RNA Delivery. *Chem. Commun.* **2011**, *47*, 8370–8372.
14. Lee, S. H.; Bae, K. H.; Kim, S. H.; Lee, K. R.; Park, T. G. Amine-Functionalized Gold Nanoparticles as Noncytotoxic and Efficient Intracellular siRNA Delivery Carriers. *Int. J. Pharm.* **2008**, *364*, 94–101.
15. Lee, J. S.; Green, J. J.; Love, K. T.; Sunshine, J.; Langer, R.; Anderson, D. G. Gold, Poly(β-amino ester) Nanoparticles for Small Interfering RNA Delivery. *Nano Lett.* **2009**, *9*, 2402–2406.
16. Davis, M. E.; Zuckerman, J. E.; Choi, C. H.; Seligson, D.; Tolcher, A.; Alabi, C. A.; Yen, Y.; Heidel, J. D.; Ribas, A. Evidence of RNAi in Humans from Systemically Administered siRNA *via* Targeted Nanoparticles. *Nature* **2010**, *464*, 1067–1070.
17. Lytton-Jean, A. K.; Langer, R.; Anderson, D. G. Five Years of siRNA Delivery: Spotlight on Gold Nanoparticles. *Small* **2011**, *7*, 1932–1937.
18. Lares, M. R.; Rossi, J. J.; Ouellet, D. L. RNAi and Small Interfering RNAs in Human Disease Therapeutic Applications. *Trends Biotechnol.* **2010**, *28*, 570–579.

19. Vita, M.; Henriksson, M. The Myc Oncoprotein as a Therapeutic Target for Human Cancer. *Semin. Cancer Biol.* **2006**, *16*, 318–330.
20. de la Fuente, J. M.; Berry, C. C. Tat Peptide as an Efficient Molecule To Translocate Gold Nanoparticles into the Cell Nucleus. *Bioconjugate Chem.* **2005**, *16*, 1176–1180.
21. Yezhelyev, M. V.; Qi, L.; O'Regan, R. M.; Nie, S.; Gao, X. Proton-Sponge Coated Quantum Dots for siRNA Delivery and Intracellular Imaging. *J. Am. Chem. Soc.* **2008**, *130*, 9006–9012.
22. Qian, S.; Zhong, X.; Yu, L.; Ding, B.; de Haan, P.; Boris-Lawrie, K. HIV-1 Tat RNA Silencing Suppressor Activity Is Conserved Across Kingdoms and Counteracts Translational Repression of HIV-1. *Proc. Natl. Acad. Sci. U.S.A.* **2009**, *106*, 605–610.
23. Sijen, T.; Fleenor, J.; Simmer, F.; Thijssen, K. L; Parrish, S.; Timmons, L.; Plasterk, R. H.; Fire, A. On the Role of RNA Amplification in dsRNA Triggered Gene Silencing. *Cell* **2001**, *107*, 465–476.
24. Tortiglione, C. An Ancient Model Organism to Test *In Vivo* Novel Functional Nanocrystals. In *Biomedical Engineering: From Theory to Application*: Fazel-Rezai, R., Ed.; InTech Publisher, 2011; pp 225−252.
25. Ambrosone, A.; Mattera, L.; Marchesano, V.; Quarta, A.; Susha, A. S.; Tino, A.; Rogach, A. L.; Tortiglione, C. Mechanisms Underlying Toxicity Induced by CdTe Quantum Dots Determined in an Invertebrate Model Organism. *Biomaterials* **2012**, *33*, 1991–2000.
26. Hartl, M.; Mitterstiller, A. M.; Valovka, T.; Breuker, K.; Hobmayer, B.; Bister, K. Stem Cell-Specific Activation of an Ancestral myc Protooncogene with Conserved Basic Functions in the Early Metazoan Hydra. *Proc. Natl. Acad. Sci. U.S.A.* **2010**, *107*, 4051–4056.
27. Ambrosone, A.; Marchesano, V.; Tino, A.; Hobmayer, B.; Tortiglione, C. Hymyc1 Downregulation Promotes Stem Cell Proliferation in *Hydra vulgaris*. *PLoS One* **2012**, *7*, e30660.
28. Semmler-Behnke, M.; Kreyling, W. G.; Lipka, J.; Fertsch, S.; Wenk, A.; Takenaka, S.; Schmid, G.; Brandau, W. Biodistribution of 1.4- and 18-nm Gold Particles in Rats. *Small* **2008**, *4*, 2108–2111.
29. Bhaskar, S.; Tian, F.; Stoeger, T.; Kreyling, W.; de la Fuente, J. M.; Grazú, V.; Borm, P.; Estrada, G.; Ntziachristos, V.; Razansky, D. Multifunctional Nanocarriers for Diagnostics, Drug Delivery and Targeted Treatment Across Blood-Brain Barrier: Perspectives on Tracking and Neuroimaging. *Part. Fibre Toxicol.* **2010**, *7*, 1–25.
30. Brooks, P. C.; Montgomery, A. M.; Rosenfeld, M.; Reisfeld, R. A.; Hu, T.; Klier, G.; Cheresh, D. A. Integrin $\alpha_v\beta_3$ Antagonists Promote Tumour Regression By Inducing Apoptosis of Angiogenic Blood Vessels. *Cell* **1994**, *79*, 1157–1164.
31. de la Fuente, J. M.; Berry, C. C.; Riehle, M. O.; Curtis, A. S. G. Nanoparticle Targeting at Cells. *Langmuir* **2006**, *22*, 3286–3293.
32. Lee, P. C.; Meisel, D. Adsorption and Surface-Enhanced Raman of Dyes on Silver and Gold Sols. *J. Phys. Chem.* **1982**, *86*, 3391–3395.
33. Adamcakova-Dodd, A.; Thorne, P. S.; Grassian, V. H. *In Vivo* Toxicity Studies of Metal and Metal Oxide Nanoparticles. In *Handbook of Systems Toxicology*; Cascinao, D. A., Sahu, S. C., Eds.; John Wiley & Sons, Ltd.: New York, 2011; pp 803−834.